Journal of Porous Materials (2019) 26:1699–1712
https://doi.org/10.1007/s10934-019-00767-1

Magnetic iron oxide modified MIL-101 composite as an efficient visible-light-driven photocatalyst for methylene blue degradation

Huynh Thi Minh Thanh[1,2] · Nguyen Thi Thanh Tu[3] · Nguyen Phi Hung[2] · Tran Ngoc Tuyen[1] · Tran Xuan Mau[1] · Dinh Quang Khieu[1]

Published online: 28 May 2019

Abstract
In this study, a facile hydrothermal method was used to prepare Fe_3O_4/MIL-101 composite as a photocatalyst. The resulting composite was characterized using X-ray diffraction, scanning electron microscopy, nitrogen adsorption/desorption isotherms, thermal analysis, X-ray photoelectron spectroscopy, and UV–Vis diffuse reflection spectroscopy. The Fe_3O_4/MIL-101 composite possesses a large surface area and mesoporous structure and exhibits a good photocatalytic activity for the MB degradation in the visible light region. A kinetic model for dye degradation over this heterogeneous catalyst was proposed by combining the parameters of the Langmuir isotherms and the kinetics of the unimolecular reaction. The proposed model fixes well with the experimental data. The mechanism of MB photocatalytic degradation is also addressed. The catalyst is stable after three recycles, which makes it a potential candidate for environmental restoration.

Keywords MIL-101 · Fe_3O_4/MIL-101 · Photocatalyst · Visible light

1 Introduction

Recently, the semiconductors have widely used as photocatalysts to degrade the organic pollutants in aquatic sources because of unique advantages including recyclable ability, taking advantage of solar energy, and low cost [1–7]. Metal–organic frameworks (MOFs) are a class of compounds consisting of metal ions or clusters coordinated to organic ligands to form one-, two-, or three-dimensional structures. They are considered as the new generation semiconductors in photocatalytic application. Primary studies on MOF-5 (Zn-benzene-1,4-dicarboxylate) have proved that benzene-1,4-dicarboxylate in MOF-5 can act as antennas to absorb light and activate zinc, which is similar to inorganic semiconductor quantum dots, via a linker to metal cluster charge transfer [8]. MIL-101, which is one of MOFs materials, has received considerable attention owing to its high surface area and porosity, well-defined structure, and chemical stability. MIL-101, reported by Férey et al. has the formula as $Cr_3X(H_2O)_2O(BDC)_3$ where X can be F or OH; BDC is benzene-1,4-dicarboxylate [9]. It is applied in sensor technology [10], gas adsorption and separation processes [11], catalysis [12, 13], and ion exchange [14]. Recently, combining functional nano and microparticles with MIL-101 in order to fabricate nano-composites with specific functional properties has attracted the interest of many researchers. In particular, the introduction of magnetic materials into MIL-101 has received considerable attention because the composites can be easily positioned by an external magnetic field. From the catalysis and adsorption point of view, magnetic separation has many more advantages compared with filtration, centrifugation, and liquid–liquid extraction [15]. Fe_3O_4/MIL-101 is reported for the efficient removal of Acid Red 1 and Orange G [16], Acid Orange 7 [17] from aqueous solutions, and a selective and regeneratable adsorbent for the removal of arsenic species from water [18]. MIL-101 plays a crucial role as a carrier in the Fe_3O_4/MIL-101 catalyst in the catalytic conversion of benzyl alcohol to benzaldehyde by enhancing the catalytic activity of Fe_3O_4 nanoparticles [19]. Fe_3O_4/MIL-101 is a highly efficient heterogeneous catalyst for the dimerization reaction of

✉ Dinh Quang Khieu
dqkhieu@hueuni.edu.vn

1 University of Sciences, Hue University, Hue 530000, Vietnam

2 Department of Chemistry, Qui Nhon University, Qui Nhon 590000, Vietnam

3 Institute for Environmental Science, Nguyen Tat Thanh University, Ho Chi Minh 700000, Vietnam

o-phenylenediamine in the presence of H_2O_2 [20]. MOF-5 (zinc-terephthalate) was reported first for photocatalytic activity. Then, more and more MOFs have found utility as novel photocatalysts [21, 22]. Several papers reported visible-light photocatalytic activity of modified MIL-101 such as N–$K_2Ti_4O_9$/MIL-101 composite [22], WO_3/MIL-101 for enhancement charge carrier separation of photocatalyst [23], Ag_3PO_4/MIL-101/$NiFe_2O_4$ composite [24], MnO_x/MIL-101 [25], and $Bi_{25}FeO_{40}$/MIL-101/PTH [26]. To the best of our knowledge, few papers have dealt with the study of the visible-light-driven photocatalytic properties of Fe_3O_4/MIL-101 up to now.

In the present paper, the synthesis of Fe_3O_4/MIL-101 is demonstrated, and the visible-light-driven-photocatalytic degradation of methylene blue using this material as a catalyst is also investigated.

2 Experimental

2.1 Materials and characterizations

Chromium nitrate hexahydrate ($Cr(NO_3)_2{\cdot}6H_2O$, Daejung, Korea, ≥ 99%), Acid Terephthalic ($C_8H_6O_4$, Merck, 99%), Iron(III) chloride hexahydrate ($FeCl_3{\cdot}6H_2O$, Daejung, Korea, 98%), Iron(II) chloride tetrahydrate ($FeCl_2{\cdot}4H_2O$, Daejung, Korea, 99%), Methanol (CH_3OH, Chemical Factory Co., Ltd. China, 99%), Methylene blue (MB) 1% ($C_{16}H_{18}N_5N_3SCl$, China) were used in this paper.

The X-ray diffraction (XRD) patterns were performed with a D8-Advance (Brucker, Germany) with Cu-Kα radiation of 0.154 nm. Infrared analyses were conducted on a BIO-RAD FTS-3000 spectrometer (Shimadzu, Japan). The textural properties of the samples were studied using nitrogen adsorption/desorption isotherms on Micromeritics ASAP 2020 (USA). The morphology was studied using scanning electron microscopy (SEM) and the elemental analyses were conducted using EDX spectroscopy on JSM Jeol 5410 LV (Japan). Transmission electron microscopy (TEM) was carried out using a JEOL JEM–2100F microscope. X-ray photoelectron spectroscopy (XPS) was performed on an ESCALab 250 (ThermoScientific Corporation, Japan) spectrometer. Magnetic measurements were conducted on a DMS 880 (ADE Technologies, USA) magnetometer with filed sweeping from − 20000 to 20000 Oe at room temperature. The photoluminescence (PL) was recorded by means of a spectrometer Horiba Jobin–Yvon HR800 LabRam using UV excitation. Raman spectra were recorded with a 750 nm laser excitation on a Horiba Raman Spectrometer. The concentration of MB was determined using a UV 1800 (Shimadzu, Japan) spectrophotometer at a maximal wavelength of 664 nm.

2.2 Synthesis of Fe_3O_4/MIL-101

MIL-101 was synthesized according to Férey et al. [9]. Typically, 1.66 g of terephthalic acid was mixed with 5 g of $Cr(NO_3)_3{\cdot}9H_2O$, 260 µL of HF, and 63 mL of distilled water. The mixture was transferred into a Teflon-lined autoclave, which was sealed and heated to 200 °C in 2 h and kept at this temperature for 8 h. After cooling to room temperature, the solid (MIL-101) was obtained by filtration, washed with ethanol, NH_4F, and N,N-dimethylformamide at 60 °C for 24 h to remove the residual terephthalic acid. The Fe_3O_4/MIL-101 material was synthesized according to Saikia et al. [19]. Practically, 1 mmol of $FeCl_2{\cdot}4H_2O$ and 2 mmol of $FeCl_3{\cdot}6H_2O$ were added to 100 mL of distilled water containing 0.5 g of MIL-101 prepared in the first experiment. The resulting suspension was stirred vigorously under a nitrogen flow for 1 h; then, 14 mL of an NH_3 solution was added. The resulting black suspension was stirred for another 30 min. After that, it was collected by centrifugation and dried at 100 °C for 24 h. The resulting product was denoted as Fe_3O_4/MIL-101. The Fe_3O_4 was synthesized for iron (II) and (III) chloride as above mentioned for the sake of comparision.

2.3 Photocatalytic degradation of MB

The photocatalytic activity of Fe_3O_4/MIL-101 was studied in the degradation of MB at ambient temperature. The adsorption of MB from aqueous solutions was performed in the dark for 300 min to ensure saturation. Then, the mixture solution continued to be stirred mechanically and visible light (60 W incandescent Lamp) was illuminated from the bottom with a cut-off filter (< 400 nm) as shown in Fig. 1. For each experiment, 0.05 g of Fe_3O_4/MIL-101 was placed in a 500 mL^3 beaker containing 300 mL^3 of dye solution (10–50 mg L^{-1}), which was stirred magnetically at 30 °C. 3 mL of the sample was withdrawn at different time intervals and determined for the MB concentration. Each determination was repeated three times. The decolorization fraction is expressed as follows:

$$F = \frac{(C_0 - C_t)}{C_0} \times 100 \quad (1)$$

where C_0 and C_t is MB concentration at initial and certain time.

The chemical oxygen demand (COD) of the MB solution was determined using the ASTM method [27]. The sample was oxidized by a boiling mixture of chromic and sulfuric acids and refluxed in a strong acid solution with a known excess of potassium dichromate. After digestion, the remaining unreacted $K_2Cr_2O_7$ was titrated with ferrous ammonium

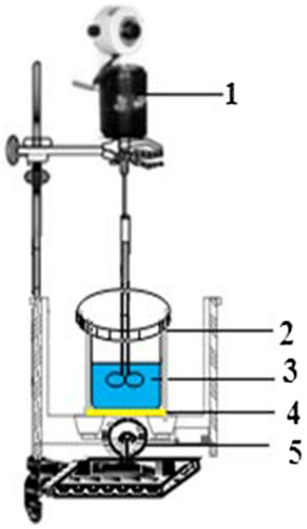

Fig. 1 Equipment for photocatalytic degradation: 1. Mechanical stirrer, 2. Aluminum paper, 3. Reactor, 4. Cut-off filter, 5. Visible light source

sulfate to determine the amount of $K_2Cr_2O_7$ consumed, and the oxidizable matter was calculated in terms of oxygen equivalent. The samples were analyzed in three measurement to yield the most reliable data.

3 Results and discussion

3.1 Characterization of Fe_3O_4/MIL–101

Figure 2a represents the XRD patterns of MIL-101 and Fe_3O_4/MIL-101. The characteristic diffractions of MIL-101 at 2θ of 5.12°; 5.85°; 8.5°; 9.1°, and 10.4° correspond to Miller index of (511), (822), (753), (1022) and (880), respectively [15, 16].These sharp peaks with high intensities indicate that the obtained MIL-101 exhibits high crystallinity [9, 15, 16]. Figure 2b presents XRD pattern of Fe_3O_4. The diffractions of Fe_3O_4 appear at Miller indices (220), (311), (400), (422), (511), and (440) (JCPDS No: 00-001-1111). The XRD pattern of Fe_3O_4/composite is composed of characteristic of Fe_3O4 and MIL-101. The results show that Fe_3O_4 is encapsulated into MIL-101 and the MIL-101 structure possesses integrity in Fe_3O_4/MIL-101 composite.

Vibration bands of FT-IR spectra at around 1398 cm^{-1} are assigned to the framework (O–C–O)-groups, confirming the presence of the dicarboxylate moieties within MIL-101 or Fe_3O_4/MIL-101 [20, 21]. The bands at around 3427 cm^{-1}, 2359 cm^{-1}, and 1624 cm^{-1} are owing to the water molecules within the frameworks [11, 12]. No vibration at 632 cm^{-1} proves no phase of hematite in nanocomposite [17, 18]. The characteristic broad band at 586 cm^{-1} for the Fe_3O_4/MIL-101 proves the incorporation of Fe–O groups on MIL-101 [20] (Fig. 2c).

The nitrogen adsorption/desorption isotherms of MIL-101 and Fe_3O_4/MIL-101 are presented in Fig. 2d. The curves belong to the H4 type according to IUPAC classification. MIL-101 has a BET (Brunauer–Emmett–Teller) surface area of 3360 $m^2\ g^{-1}$ and a pore volume of 1.43 $cm^3\ g^{-1}$. Fe_3O_4/MIL-101 has a lower BET surface area and pore volume than the parent material because the pores of the parent material are filled with Fe_3O_4 particles. However, a significant BET surface area of 1860 $m^2\ g^{-1}$ and pore volume of 0.72 $cm^3\ g^{-1}$ are conserved. This also proves the encapsulation of iron oxides within the pores of the framework.

The TGA and DTA curves of Fe_3O_4/MIL-101 exhibit two main weight losses: the first in the temperature range of 25–118 °C corresponds to the loss of the physically adsorbed water and the second between 118 and 375 °C is associated with the decomposition of the organic framework with an exothermic peak at 375.89 °C (Fig. 2e).

The morphology of MIL-101 and Fe_3O_4/MIL-101 was observed using SEM (Fig. 3a, b). Pure MIL-101 shows 0.5 µm octahedral shape particles with smooth facets, while Fe_3O_4/MIL-101 provides the octahedral particles with rough facets because the fine particles of Fe_3O_4 with 10–20 nm size are incorporated into the MIL-101 surface (Fig. 3c). The elementary analysis by means of EDX shows the presence of iron and chromium in the Fe_3O_4/MIL-101 composite (Fig. 3d). Since the results of EDX only reflect the surface composition of the elements, the molar ratio of Fe/Cr (1.27/1) is significantly higher than that of the initially synthesized gel (0.38/1), indicating that iron is introduced into MIL-101 and located mainly on the surface the crystals. No typical hysteresis loop of the Fe_3O_4/MIL-101 nanocomposite is observed, suggesting the superparamagnetic behavior of the material owing to the aggregation of the small-sized spherical magnetic particles (Fig. 3e). The saturation magnetization value of the nanocomposite is around 15 emu g^{-1}. This value is small compared with that of the Fe_3O_4 nanoparticles due to the small particle size effect and the presence of the non-magnetic MIL-101 support in the nanocomposite. This superparamagnetic behavior of the Fe_3O_4/MIL-101 composite allows the particles to aggregate rapidly in the presence of an external magnetic field. However, the particles disperse easily as soon as the external field is removed.

The elemental composition and oxidation states of the metals were studied using X-ray photoelectron spectroscopy (XPS). The XPS survey spectrum shows that C, O, Cr, and Fe exist in Fe_3O_4/MIL-101 (Fig. 4a). Figure 4d demonstrates the high-resolution XPS spectrum of C1s, which can be deconvoluted into two surface components, corresponding to the carbon components on the benzoic ring at a binding energy of 284.6 eV and the carboxylate (C=O) groups of the

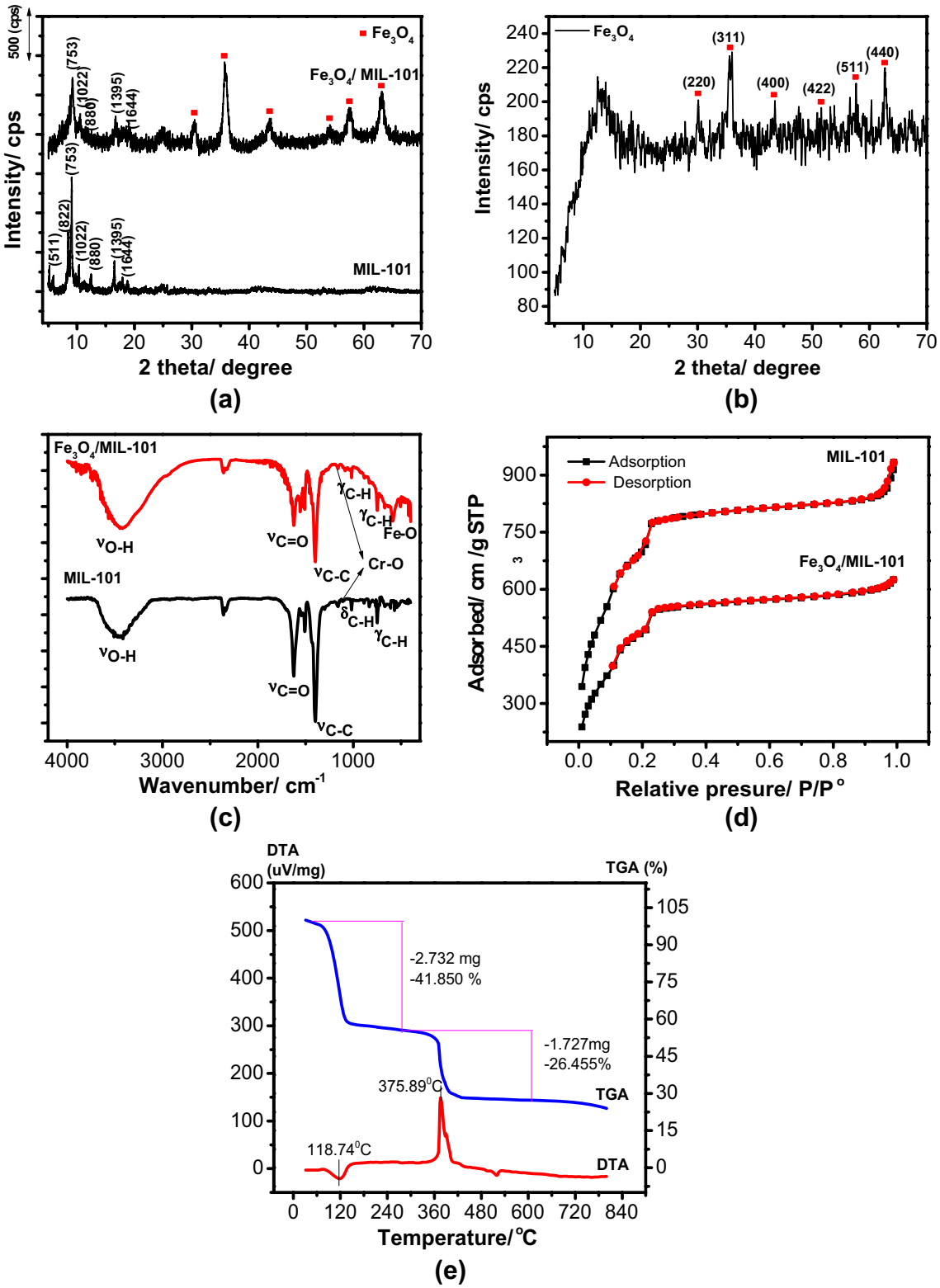

Fig. 2 XRD patterns of MIL-101 and Fe_3O_4/MIL-101 composite (**a**); Fe_3O_4 (**b**); FT-IR spectra (**c**), nitrogen adsorption/desorption isotherms (**d**) of MIL-101 and Fe_3O_4/MIL-101 composite; TG–DTA curves of Fe_3O_4/MIL-101 composite (**e**)

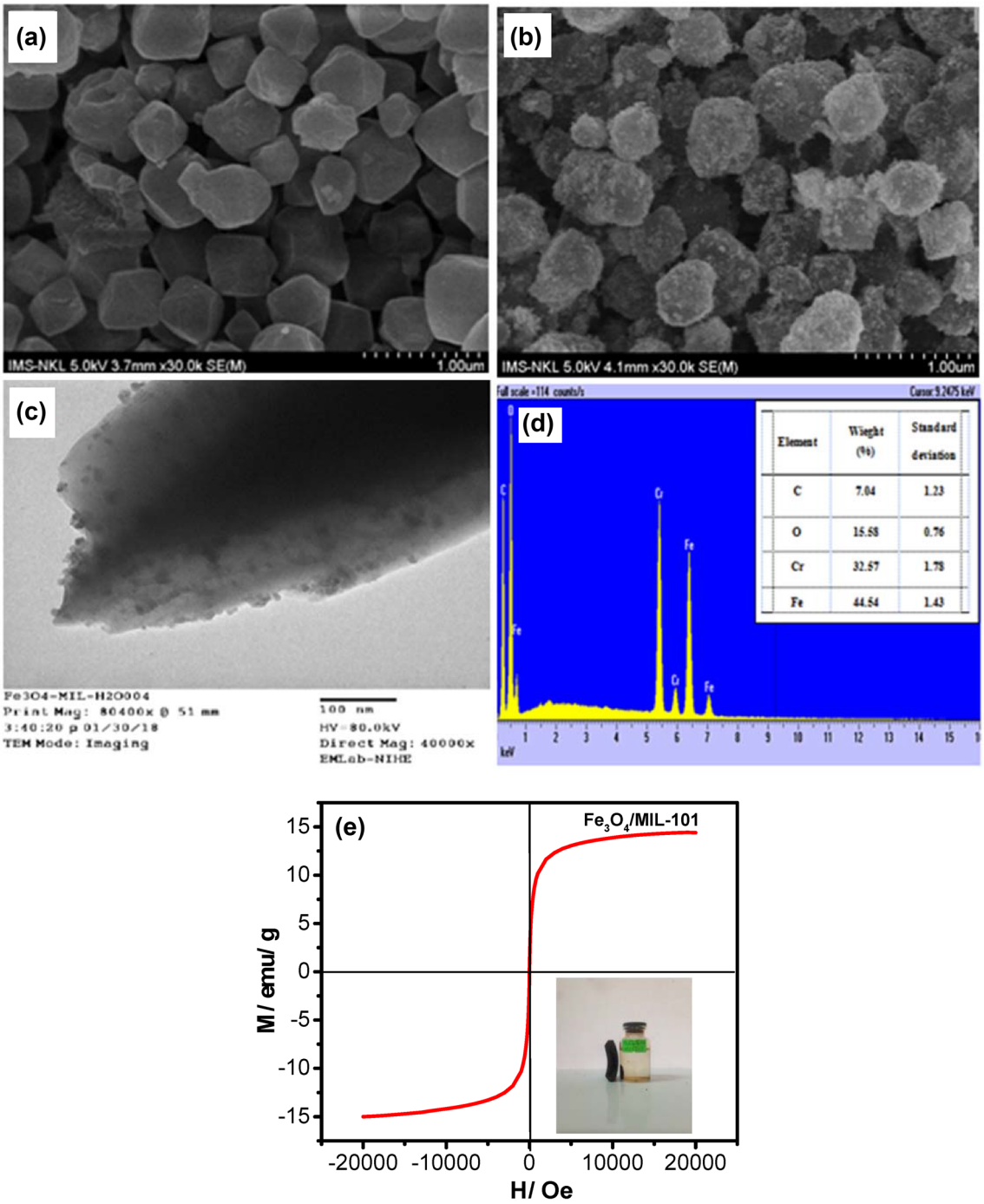

Fig. 3 SEM observation of MIL-101 (**a**) and Fe_3O_4/MIL-101 (**b**); TEM observation of Fe_3O_4/MIL-101 (**c**); EDX spectrum of Fe_3O_4/MIL-101 (**d**); magnetic hysteresis loops of Fe_3O_4/MIL-101 (**e**)

terephthalate linkers at a binding energy of 288.6 eV [21, 28]. The XPS spectrum of O1s could be fitted by two peaks at binding energies of around 531.7 and 530.4 eV (Fig. 4e), which are assigned to the oxygen components on terephthalate linkers and on the iron oxide, respectively [22, 23]. For the Fe2p spectrum (Fig. 4b), the binding energy peak around 714.4 eV is contributed to Fe2p3/2 and the peak at 725.8 eV is contributed to Fe2p1/2. All of these results clearly confirm the formation of Fe_3O_4/MIL-101. The binding energy values of 585.8 eV for Cr2p1/2 and 576.3 eV for Cr2p3/2 (Fig. 4c) are typically assigned to Cr(III) [29].

The photoluminescence (PL) emission spectrum has widely been employed to study the efficiency of charge carrier trapping, immigration, and transfer [30–32]. In

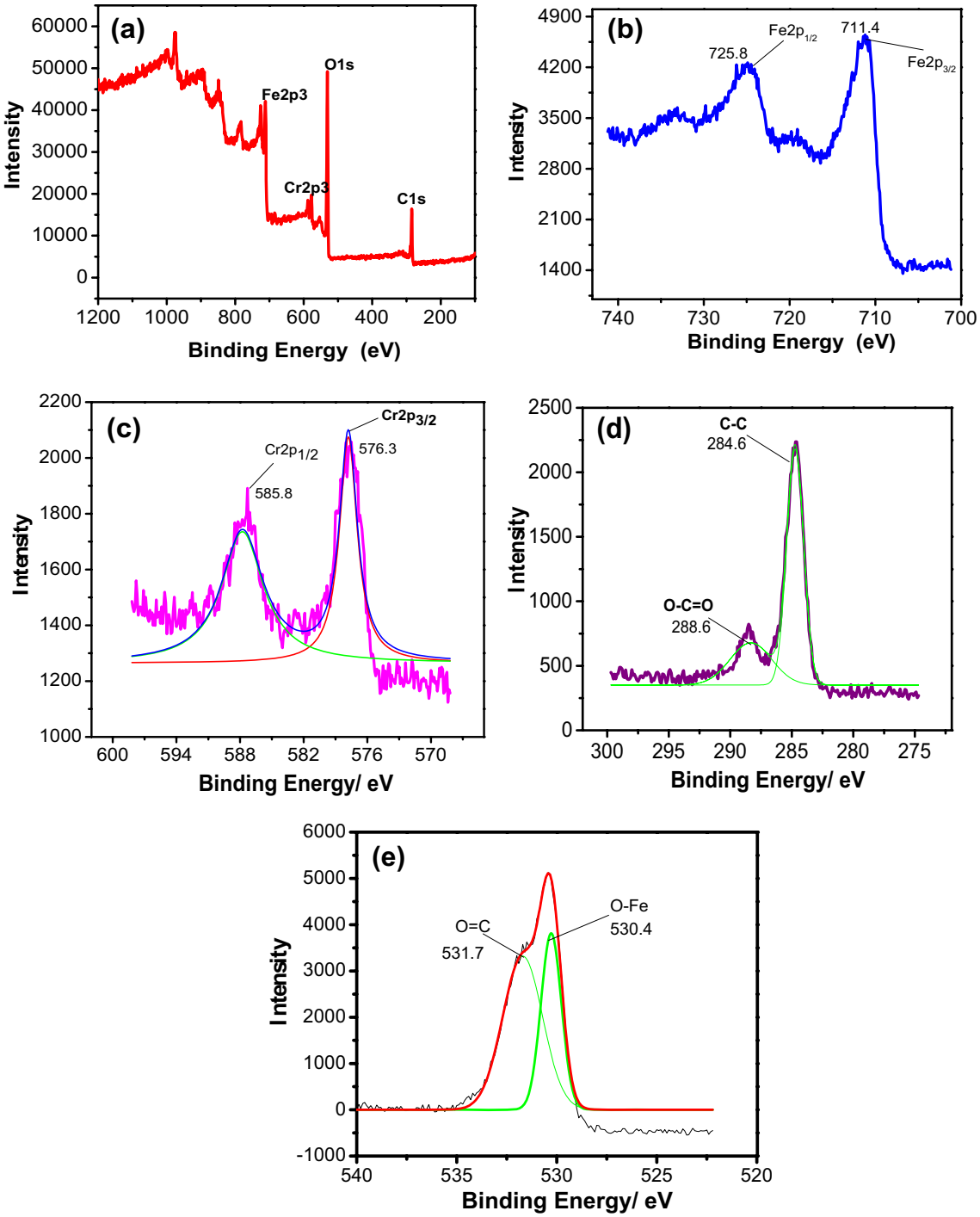

Fig. 4 XPS spectra of Fe_3O_4/MIL-101: **a** survey spectrum; **b** Fe2p; **c** Cr2p; **d** C1s; **e** O1s

order to study the effect of Fe_3O_4 on the recombination of electron–hole pairs produced by MIL-101. The PL presented in Fig. 5a compares electron–hole recombination of Fe_3O_4/MIL-101 and MIL-101. MIL-101 shows a broad PL emission band, which is similar to that in the literature [33]. Fe_3O_4/MIL-101 shows diminished PL intensity, implying lower charge recombination in comparison with pure MIL-101. Peak shifting from 392 nm for MIL-101 to 400 nm for Fe_3O_4/MIL-101 is resulted from the trapping of electrons at defect sites prior to recombination [34]. Raman spectra were employed to study the structure and surface defects of semiconductors [35]. We did not observe obvious peak shifts for the MOF bands in the Raman spectra. The two sharp peaks at 1618 and

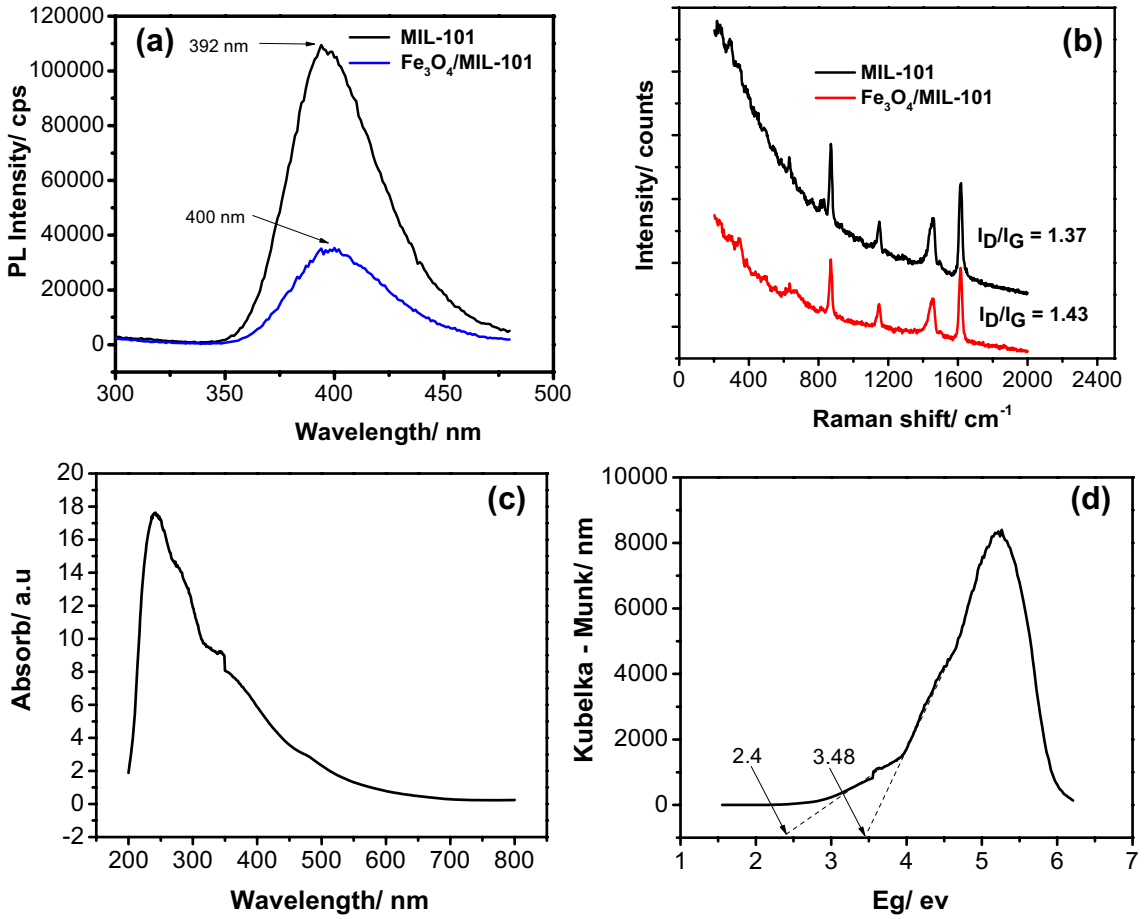

Fig. 5 **a** PL spectra of MIL-101 and Fe_3O_4/MIL-101; **b** Raman spectra of MIL-101 and Fe_3O_4/MIL-101; **c** UV–Vis DRS; **d** Kubelka–Munk plot of Fe_3O_4/MIL-101

1461 cm^{-1} correspond to the D and G bands, respectively [36, 37]. The intensity ratio of the D and G bands (I_D/I_G) is used to estimate the disorder in the materials. It is found that the I_D/I_G ratio of Fe_3O_4/MIL-101 (1.43) is higher than that of pure MIL-101 (1.37), which implies that magnetic iron oxide has successfully been tailored in Fe_3O_4/MIL-101 (Fig. 5b). The UV–Vis diffuse reflection spectrum is widely used to calculate the optical band gap energy [2, 3, 6, 7]. The band gaps of the Fe_3O_4/MIL-101 composite were studied by means of a UV–Vis diffuse reflection spectrum at room temperature (Fig. 5c). Fe_3O_4/MIL-101 shows an absorption edge around 200–600 nm (Fig. 5c). A very high absorption peak around 230 nm indicates the $\pi \rightarrow \pi^*$ transitions in the terephthalate ring. Fe_3O_4/MIL-101 shows a remarkable absorption band shifting towards the longer wavelength region. The band gaps obtained from the Kubelka–Munk plot are 3.48 and 2.4 eV (Fig. 5d). The observed decrease in the band gap energy of the iron-doped MIL-101 may be attributed to the excitation of the 3d electrons of Fe(III) or Fe(II) to the conduction band level of Cr by a charge transfer transition. The low band gap at 2.4 eV enables Fe_3O_4/MIL-101 to exhibit the photocatalytic activity under visible light.

3.2 Visible-light-driven photocatalytic degradation of MB over Fe_3O_4/MIL-101

3.2.1 Catalytic kinetics

Figure 6a shows the decolorization fraction for MB in dark adsorption and under the visible light illumination with and without the catalyst. The MB solution was not decolorized under visible light in the absence of MIL-101 and Fe_3O_4/MIL-101, indicating that the photolysis of MB under this condition could be ignored. MIL-101 exhibits a higher adsorption capacity than Fe_3O_4/MIL-101 with the equilibrium decolorization fraction at 73.5% and 57.3% in dark adsorption, respectively. However, the MB solution decolorizes up to 95% with Fe_3O_4/MIL-101 after 650 min of illumination; meanwhile, the decolorization is not observed in the MB solution containing MIL-101 under the same condition. This suggests that MIL-101

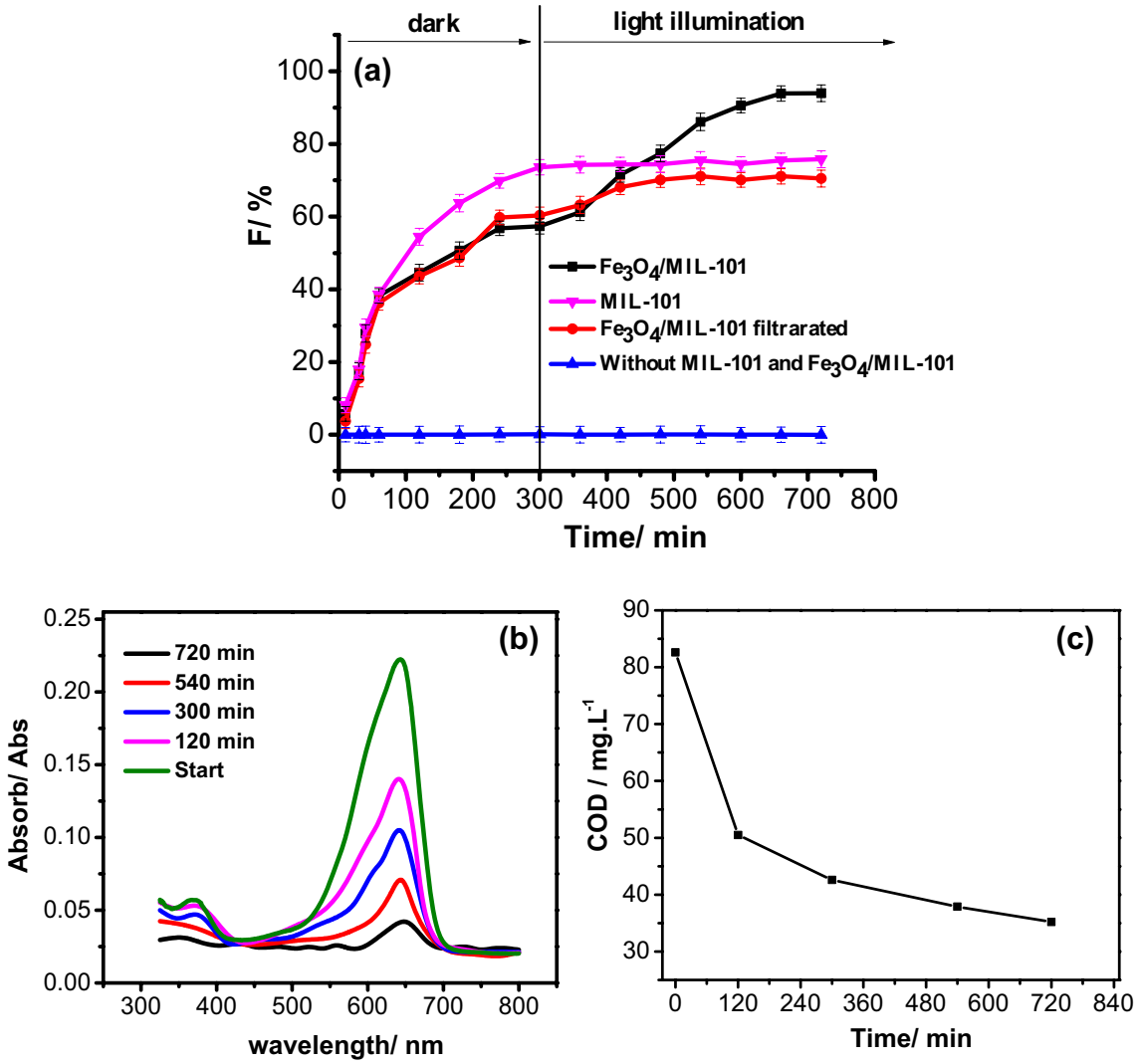

Fig. 6 **a** The decolorization of MB under the illumination of visible light, with and without MIL-101 and Fe_3O_4/MIL-101; **b** UV–Vis spectra; **c** COD value (conditions: $C_0 = 31.38$ mg L^{-1}, $V = 100$ mL, $m_{Cat} = 0.05$ g)

is not a photocatalyst for MB degradation. The leaching experiment, in which Fe_3O_4/MIL-101 was filtered after 420 min, was also conducted. The decolorization of MB does not take place under illumination, confirming that Fe_3O_4/MIL-101 is a heterogeneous photocatalyst in the degradation of MB.

The UV–Vis spectra for the photocatalytic degradation of MB over Fe_3O_4/MIL-101show that the adsorption band peaks at 664 nm (electron transfer $\pi \rightarrow \pi^*$ in the MB structure), and the concentration of MB in the solution decreases with illumination time (Fig. 6b).

To confirm the mineralization of MB over Fe_3O_4/MIL-101, the change of COD of the reaction products with time was analyzed. The initial COD of 82.6 mg L^{-1} decreases with the illumination reaching 35.2 mg L^{-1} after 720 min (Fig. 6c). This decrease proves that Fe_3O_4/MIL-101 is an efficient photocatalyst for MB degradation under visible light.

There are two common approaches for investigating formal kinetics of heterogeneous catalytic reactions: (i) the light illumination is performed as soon as the catalyst is included; (ii) the light illumination is performed only when the catalyst adsorbs at saturation in the dark. There is a difficulty to distinguish the adsorption and catalysis processes in the first approach. This problem is solved in the second approach, but it is difficult to determine the initial concentration of the catalyst in the kinetic equation. In this case, the initial concentration is considered as the equilibrium concentration in dark adsorption. Very few articles [38] have dealt with this issue so far.

It is known that the Langmuir–Heishellwood model is widely used to study the formal kinetics of dye degradation over heterogeneous photocatalysts. This model is as follows:

$$\ln \frac{C_t}{C_0} = -k_1 \times t \tag{2}$$

where k_1 is rate constant (min^{-1}); C_0 and C_t are MB concentration at initial and time t (mg L^{-1}).

In the present study, we propose a modified Langmuir–Heishellwood model, in which the Langmuir equilibrium constant and the kinetics are combined.

Figure 7a presents the kinetics of adsorption and photocatalytic decolorization of MB over Fe_3O_4/MIL-101. Fe_3O_4/MIL-101 exhibits a high adsorption capacity of MB. The adsorption is saturated between 240 and 300 min depending on the initial MB concentration. The higher the MB concentration causes the slower saturation. After 300 min, the adsorption ensures saturation.

The equilibrium adsorption capacity, q_e, is expressed as follows:

$$q_e = \frac{V \times (C_0 - C_e)}{m} \tag{3}$$

where C_0 and C_e are the MB concentration at initial and equilibrium time (mg L^{-1}); V is the volume of the MB solution (L); m is the mass of catalyst (g).

The relationship between C_e and q_e is expressed by the Langmuir isotherm model [38]:

$$q_e = \frac{K_L \times q_m \times C_e}{1 + K_L \times C_e} \tag{4}$$

where q_m is the maximum monolayer adsorption capacity (mg L^{-1}); K_L is the Langmuir adsorption equilibrium constant (mg L^{-1}).

The value of K_L and q_m can be obtained from the slope and intercept of the linear plot of $1/C_e$ versus q_e. A high determination coefficient ($R^2 = 0.97$) shows that this model could fix the experimental data well, and implies the monolayer adsorption on the adsorbents. The values of q_m and K_L are 243.6 mg g^{-1} and 0.013 L mg^{-1}, respectively.

It is supposed that MB molecules adsorb on the catalyst and then they degrade on the catalyst surface under visible light illumination. The overall reaction could be illustrated as follows:

$$Fe_3O_4/01 + MB \underset{k_{-1}}{\overset{k_1}{\rightleftharpoons}} \left(Fe_3O_4/\text{MIL-101} \ldots MB\right)^* \xrightarrow{k_2} \text{products}$$

where k_1 is the forward adsorption rate constant; k_{-1} is the back adsorption rate constant; k_2 is the photocatalytic rate coefficient.

It is supposed that the photocatalytic degradation is slow and is the rate-determining step. Therefore, the law rate is expressed as follows:

$$r = -\frac{dC}{dt} = k_2 \times \theta \tag{5}$$

where C is the dye concentration (mg L^{-1}) at time t; k_2 is the kinetics rate coefficient (mg L^{-1} min^{-1}); θ is the fraction of the surface covered by MB. θ is expressed in the Langmuir model [39]:

$$\theta = \frac{K_L \times C}{1 + K_L \times C} \tag{6}$$

Substituting (6) to (5) gives

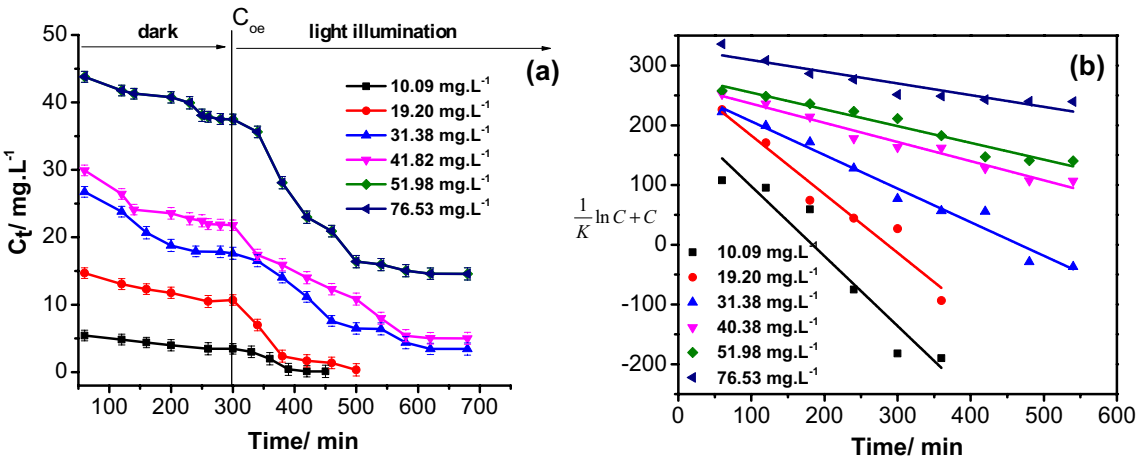

Fig. 7 **a** Adsorption and photocatalytic decolorization kinetics of MB over Fe_3O_4/MIL-101 in dark and under visible light; **b** modified Langmuir–Hinshelwood's plot at different initial concentrations of catalyst (conditions: $C_0 = 31.38$ mg L^{-1}, $V = 100$ mL, $m_{Cat} = 0.05$ g)

$$\frac{dC}{dt} = -k_2 \times \frac{K_L \times C}{1 + K_L \times C} \tag{7}$$

Then,

$$\int \frac{1 + K_L \times C}{K_L \times C} \times dC = -\int k_2 \times dt \tag{8}$$

Integrating Eq. (8) with the boundary conditions $t \rightarrow 0$ and $C \rightarrow C_{0e}$ gives

$$\frac{1}{K_L} \times \ln C + C = -k_2 \times t + I_0 \tag{9}$$

When $t = 0$, then

$$I_0 = \frac{1}{K_L} \times \ln C_{0e} + C_{0e} \tag{10}$$

Substituting (10) into (9) gives

$$\frac{1}{K_L} \times \ln C + C = -k_2 \times t + \frac{1}{K_L} \times \ln C_{0e} + C_{0e} \tag{11}$$

where K_L is the Langmuir adsorption equilibrium constant (L mg^{-1}), which is determined from the Langmuir isotherm model as above; C_{0e} (mg L^{-1}) is the equilibrium concentration of adsorbate at time t (min) taken from light illumination.

The plot of the $\frac{1}{K} \ln C + C$ against t gives a straight line with slope k_2 (Fig. 7b).

The kinetics data are fixed to the Langmuir–Hinshelwood model for the sake of comparison. The value of k_2 at different initial MB concentrations is listed in Table 1. The coefficient of determination of the straight lines is higher than those of the Langmuir–Hinshelwood model ($t(5) = 2.597$, p value $= 0.048 < 0.05$), indicating the proposed modified Langmuir–Hinshelwood model has a goodness of fix for the experimental data. The value of k_2 decreases with the increase of the initial MB concentration. A higher MB concentration can shield the light from interacting with the catalyst, resulting in a lower rate coefficient.

It is difficult to compare the catalytic activity of Fe_3O_4/MIL-101 composite in the present with that of other catalysts previously reported due to different reaction conditions. The pseudo-first-order rate constant of Langmuir–Hinshelwood model seems appropriate to compare the catalytic activity because several authors report this value (Table 2). The value of the pseudo-first -order rate constant for the degradation on the present catalyst in the visible region is lower than that for P25 (TiO_2) in the UV region and compatible with Ce–TiO_2, but higher than that for other catalysts reported such as Ag–ZnO and Ce–TiO_2 in visible region. This result shows that the photocatalytic activity of Fe_3O_4/MIL-101 is relatively high.

Table 1 The value of k_2 at different initial MB concentration

Concentration (mg L^{-1})	Modified Langmuir–Hinshelwood model		Langmuir–Hinshelwood model	
	k_2 (mg L^{-1} min^{-1})	R^2	k_1 (min^{-1})	R^2
10.09	1.169	0.971	0.0301	0.921
19.2	0.981	0.975	0.0136	0.932
31.38	0.562	0.970	0.00641	0.960
40.38	0.320	0.968	0.00349	0.950
51.98	0.280	0.951	0.00299	0.940
76.53	0.195	0.955	0.00185	0.845

3.2.2 Mechanism of heterogeneous catalyst

To figure out the mechanisms of photocatalytic activity, radical scavengers such as *tert*-butanol (TB), 1,4-benzoquinone (BQ), dimethyl sulfoxide (DMSO), and ammonium oxalate (AO) were used to quench hydroxyl radicals

Table 2 Comparion of pseudo-first-order rate constant of the present catalyst with published articles

Catalyst	BET specific surface area (m^2 g^{-1})	Light source (nm, power)	Co (mg L^{-1})/volume (mL)/$m_{catalyst}$ (mg)	Pseudo-first-order rate constant k (min^{-1})	References
ZnO	8.21	UV, 20	10/100/50	0.022	[40]
Prinstine TiO_2 (P25)	–	254, 11 W	10/100/50	0.09	[41]
Ce–TiO_2	46	370, 18 W	9.60/100/50	0.025	[42]
TiO_2	50	340, 125 W	23/2750/375	0.025	[43]
CdS	111.2	> 420, 500 W	25/200/80	0.0079	[44]
g-C_3N_4	9.8	> 420, 500 W	25/200/80	0.0039	[44]
g-C_3N_4–CdS	166.5	> 420, 500 W	25/200/80	0.0121	[44]
Ag/ZnO	–	> 570, (high pressure sodium lamp)	5/–/150	0.00547	[45]
Ta–ZnO	36	> 420, 300	10/50/50	0.0401	[46]
Fe_3O_4/MIL-101	1860	> 380, 60 W incandescent Lamp	10.09/100/0.05	0.0301	The present work

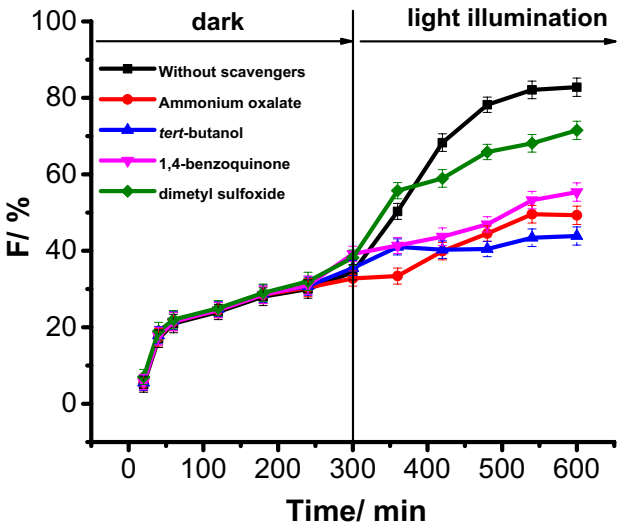

Fig. 8 Effects of radical scavengers on the degradation efficiency of methylene blue (conditions: $C_{scavenger}=10$ mmol L^{-1}, $V_{scavenger}=2$ mL, $m_{Cat}=0.05$ g, $C_0=31.38$ mg L^{-1})

(·OH), superoxide radicals ($^{-}O_2$), e^- and h^+, respectively. The mixture of MB solution and the catalyst was stirred for 300 min to ensure adsorption/desorption equilibrium and then the scavenger solution was added as soon as the light was turned on. As seen in Fig. 8, the MB degradation rate tends to decrease as the corresponding radical scavenger is added to the reaction solution. AO and TB decrease the MB degradation rate significantly. After 600 min reaction, the MB decolorization fraction reaches 82% for the case without radical scavengers, and it only reaches 49.5% for AO and 43.8% for TB. Meanwhile, BQ and DMSO slightly slow down the degradation rate of MB. These findings imply that ·OH and h^+ play a critical role in MB degradation although $^{-}O_2$ and e^- contribute to MB degradation as well.

The general coupled semiconductor mechanism [6, 7, 34, 45] could be manipulated to explain the MB degradation over the Fe_3O_4/MIL-101 catalyst. The edge of the valence band (VB) and conduction band (CB) for MIL-101 is +0.49 eV, and −1.57 eV, respectively [47], and for Fe_3O_4 is 0.48 and 2.08 eV [48], respectively. Firstly, MB molecules adsorb quickly onto Fe_3O_4/MIL-101 to form MB_{ads} (reaction (12)). Both MIL-101 and Fe_3O_4 could absorb visible light to generate the pairs of e^- and h^+ at CB and VB, respectively, according to reaction (13). CB of MIL-101 is more negative than that of Fe_3O_4, then it will transfer the excited electrons to CB of Fe_3O_4 that is believed to prevent the fast recombination of the photo-excited e^- and h^+ pairs. The LUMO (lowest unoccupied molecular orbital) of photo-excited MB· (–3.81 eV) is more negative than CB of Fe_3O_4 [49]. Therefore, MB could act as the photosensitizer to favorably provide additional photogenerated electrons into CBs of Fe_3O_4 through the formed downstream channel (reaction (14) and (15)). The energy of h^+ of Fe_3O_4 (2.08 V) is more positive than the potential of H_2O/OH· (+1.9 V) [50]. Then, h^+ could be quickly converted to the hydroxyl radical upon oxidation of surface water, according to reaction (16). The potential of e^- in MIL-101 (–1.57 V) is more negative than that of $O_2/^{-}O_2$ (–0.28 V), then introduced oxygen forms the free radicals $^{-}O_2$, as reaction (17). These radicals are responsible for MB degradation (reaction (18) and (19)). According to the published articles [49, 50], the reactions could be illustrated as follows (see Fig. 9):

$$Fe_3O_4/\text{MIL-101} + \text{MB} \rightarrow \text{MB}_{(ads)} \rightarrow \text{MB}^{\cdot}_{(ads)} \quad (12)$$

$$Fe_3O_4/\text{MIL-101} + h\nu \rightarrow Fe_3O_4/\text{MIL-101}\,(e^- + h^+) \quad (13)$$

$$\text{MB}^{\cdot} \rightarrow e^- + \text{MB}^{\cdot+} \quad (14)$$

$$\text{MB}^{\cdot+} \rightarrow \text{MB} + h^+ \quad (15)$$

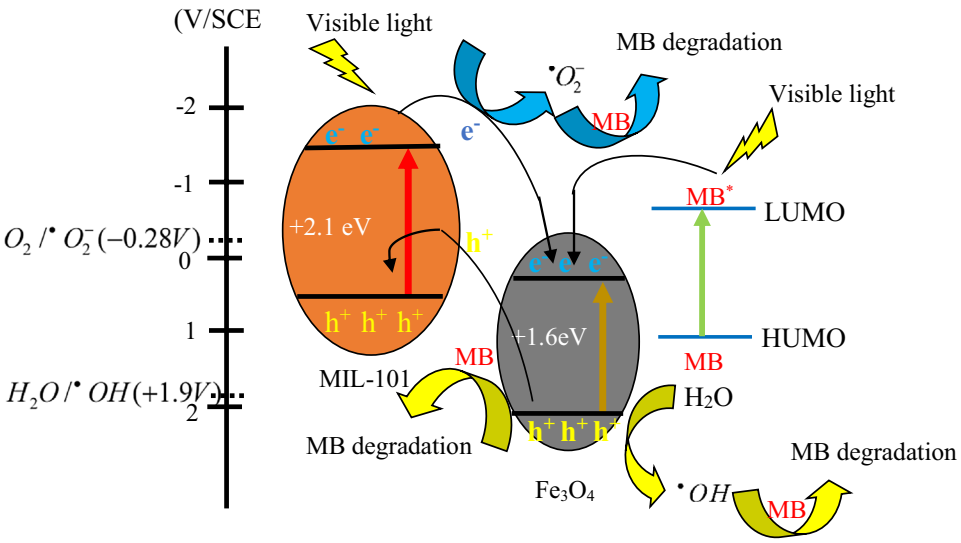

Fig. 9 Proposed mechanism of MB degradation

$$Fe_3O_4(h^+) + H_2O \rightarrow OH^{\cdot} \quad (16)$$

$$MIL\text{-}101(e^-) + O_{2(ads)} \rightarrow {}^{-\cdot}O_2 \quad (17)$$

$$^{\cdot}OH + MB_{(ads)} \rightarrow \text{Degradation products} \quad (18)$$

$$Fe_3O_4(h^+) + MB_{(ads)} \rightarrow \text{Degradation products} \quad (19)$$

$$^{-\cdot}O_2 + MB(ads) \rightarrow \text{Degradation products} \quad (20)$$

To evaluate the reusability of Fe_3O_4/MIL-101 for catalyzing MB degradation, the used Fe_3O_4/MIL-101 was regenerated by drying for 24 h at 100 °C and then reused. The catalytic activities of the reused Fe_3O_4/MIL-101 are presented in Fig. 10. The COD of the initial MB solution is 85.2 mg L^{-1}. After 720 min of adsorption and illumination, COD reduces to 35.9 mg L^{-1}. After the second, third and fourth cycle, COD reduces to 37.2, 39.8, and 39.9 mg L^{-1} (Fig. 10a). Although the photo-catalytic activity decreases gradually with an increase in cycles, the regenerated Fe_3O_4/MIL-101 still remained good performance for its catalytic activity. The Fe_3O_4/MIL-101catalyst after the fourth use shows an XRD pattern with the decreasing characteristic peaks in comparison with the original catalyst (Fig. 10b). This indicates the stability and true heterogeneous nature of the catalyst under the experimental conditions.

In addition, the Fe_3O_4/MIL-101 catalyst reveals excellent photocatalytic degradation of several other dyes (Congo Red (CR), Methyl Orange (MO), and Rhodamine-B (RD) (Fig. 11). The results found above show that Fe_3O_4/MIL-101 is a promising photocatalyst for the treatment of organic pollutants in aqueous solutions.

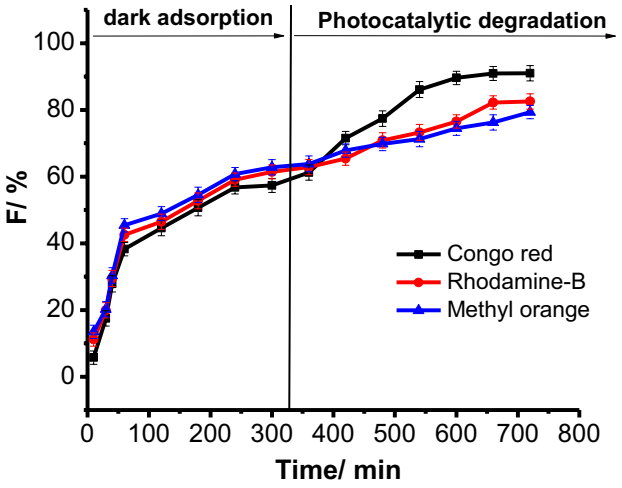

Fig. 11 Visible-light-driven photocatalytic degradation of several dyes over Fe_3O_4/MIL-101 (Conditions: C_{CR} = 30.28 mg L^{-1}; C_{RD} = 28.76 mg L^{-1}; C_{MO} = 30.15 mg L^{-1}; V = 100 mL; m_{Cat} = 0.05 g; illumination time = 420 min)

4 Conclusions

Highly active Fe_3O_4/MIL-101composite with large surface area, mesoporous heterostructures, and enhanced visible-light absorption was successfully prepared on the basis of hydrothermal strategy where MIL-101 acts as the semiconductor for the formation of catalytic heterostructures. Fe_3O_4/MIL-101 is a heterogeneous catalyst in nature and stable after the fourth reuse. We proposed a kinetic model of dye degradation over this heterogeneous catalyst by combining the parameters of Langmuir isotherms and kinetics of the

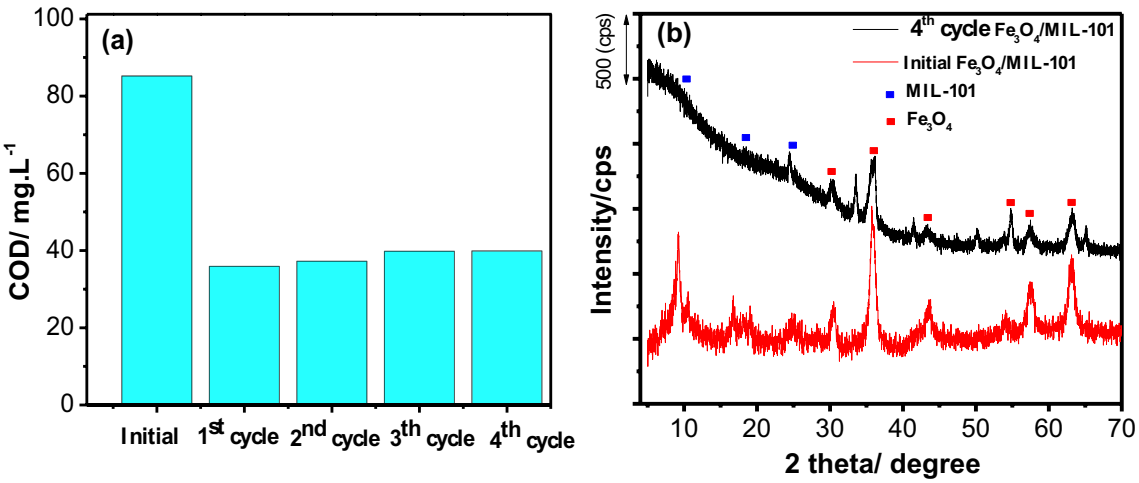

Fig. 10 **a** COD value of MB solution after four recyles; **b** XRD patterns of Fe_3O_4/MIL-101 after three cycles; (Conditions: C_0 = 31.38 mg L^{-1} (COD = 31.38 mg L^{-1}); V = 100 mL; m_{Cat} = 0.05 g)

unimolecular reaction. This model exhibits goodness of fit for the kinetics data.

Acknowledgements This research was sponsored by Hue University under Decision No. 1208/QĐ-DHH.

References

1. H. Safajou, H. Khojasteh, M. Salavati-Niasari, S. Mortazavi-Derazkola, Enhanced photocatalytic degradation of dyes over graphene/Pd/TiO_2 nanocomposites: TiO_2 nanowires versus TiO_2 nanoparticles. J. Colloid Interface Sci. **498**, 423–432 (2017)
2. M. Ghanbari, M. Salavati-Niasari, Tl_4CdI_6 nanostructures: facile sonochemical synthesis and photocatalytic activity for removal of organic dyes. Inorg. Chem. **57**, 11443–11455 (2018)
3. M. Ghanbari, F. Ansari, M. Salavati-Niasari, Simple synthesis-controlled fabrication of thallium cadmium iodide nanostructures via a novel route and photocatalytic investigation in degradation of toxic dyes. Inorgan. Chim. Acta **455**, 88–97 (2017)
4. S. Zinatloo-Ajabshir, M. Salavati-Niasari, M. Hamadanian, Praseodymium oxide nanostructures: novel solvent-less preparation, characterization and investigation of their optical and photocatalytic properties. RSC Adv. **5**, 33792–33800 (2015)
5. S. Zinatloo-Ajabshir, M. Salavati-Niasari, Nanocrystalline Pr_6O_{11}: synthesis, characterization, optical and photocatalytic properties. New J. Chem. **39**, 3948–3955 (2015)
6. S. Zinatloo-Ajabshir, M. Salavati-Niasari, Facile route to synthesize zirconium dioxide (ZrO_2) nanostructures: structural, optical and photocatalytic studies. J. Mol. Liq. **216**, 545–551 (2016)
7. S. Zinatloo-Ajabshir, M.S. Morassaei, M. Salavati-Niasari, Facile fabrication of $Dy_2Sn_2O_{72}$ nanocomposites as an effective photocatalyst for degradation and removal of organic contaminants. J. Colloid Interface Sci. **497**, 298–308 (2017)
8. T. Tachikawa, J.R. Choi, M. Fujitsuka, T. Majima, MOF-5 Tachikawa.pdf, J. Phys. Chem, C **112**, 14090–14101 (2008)
9. G. Férey, C. Mellot-Draznieks, C. Serre, F. Millange, J. Dutour, S. Surblé, I. Margiolaki, A chromium terephthalate-based solid with unusually large pore volumes and surface area. Science **309**, 2040–2042 (2005)
10. L.E. Kreno, K. Leong, O.K. Farha, M. Allendorf, R.P. Van Duyne, J.T. Hupp, Metal–organic framework materials as chemical sensors. Chem. Rev. **112**, 1105–1125 (2012)
11. H.B.T. Jeazet, C. Staudt, C. Janiak, A method for increasing permeability in O_2/N_2 separation with mixed-matrix membranes made of water-stable MIL-101 and polysulfone. Chem. Commun. **48**, 2140–2142 (2012)
12. A. Corma, H. García, F.X. Llabrés i Xamena, Engineering metal organic frameworks for heterogeneous catalysis. Chem. Rev. **110**, 4606–4655 (2010). https://doi.org/10.1021/cr9003924
13. N.T.S. Phan, T.T. Nguyen, Q.H. Luu, L.T.L. Nguyen, Paal-Knorr reaction catalyzed by metal-organic framework IRMOF-3 as an efficient and reusable heterogeneous catalyst. J. Mol. Catal. A **363–364**, 178–185 (2012)
14. K.S. Min, M.P. Suh, Silver(I)-polynitrile network solids for anion exchange: anion-induced transformation of supramolecular structure in the crystalline state. J. Am. Chem. Soc. **122**, 6834–6840 (2000)
15. P.N. Dave, L.V. Chopda, Application of iron oxide nanomaterials for the removal of heavy metals. J. Nanotechnol. **2014**, 1–14 (2014)
16. T. Wang, P. Zhao, N. Lu, H. Chen, C. Zhang, X. Hou, Facile fabrication of Fe_3O_4/MIL-101(Cr) for effective removal of acid red 1 and orange G from aqueous solution. Chem. Eng. J. **101**, 1–50 (2016)
17. X. Yue, W. Guo, X. Li, H. Zhou, R. Wang, Core-shell Fe_3O_4@MIL-101(Fe) composites as heterogeneous catalysts of persulfate activation for the removal of acid orange 7. Environ. Sci. Pollut. Res. **101**, 1629–1658 (2016)
18. K. Folens, K. Leus, N.R. Nicomel, M. Meledina, S. Turner, G. Van Tendeloo, G. Du Laing, P. Van Der Voort, Fe_3O_4@MIL-101—a selective and regenerable adsorbent for the removal of as species from water. Eur. J. Inorg. Chem. **2016**, 4395–4401 (2016)
19. M. Saikia, D. Bhuyan, L. Saikia, Facile synthesis of Fe_3O_4 nanoparticles on metal organic framework MIL-101(Cr): characterization and catalytic activity. New J. Chem. **39**, 64–67 (2015)
20. Z.W. Jiang, Y.F.L. Fu Qiang Dai, C.Z. Huang, Facile synthesis of Fe_3O_4/MIL-101(Fe) composite with enhanced catalytic performance. RSC Adv. **1**, 1–3 (2016)
21. L. Shen, S. Liang, W. Wu, R. Liang, L. Wu, CdS-decorated UiO–66(NH_2) nanocomposites fabricated by a facile photodeposition process: an efficient and stable visible-light-driven photocatalyst for selective oxidation of alcohols. J. Mater. Chem. A **1**, 11473–11482 (2013)
22. Y. Xu, Q. Chen, H. Yang, M. Lv, Q. He, X. Liu, F. Wei, Enhanced photodegradation of Rhodamine B under visible light by N-$K_2Ti_4O_9$/MIL-101 composite. Mater. Sci. Semicond. Process. **36**, 115–123 (2015)
23. L. Wang, L. Zan, WO_3 in suit embed into MIL-101 for enhancement charge carrier separation of photocatalyst. Sci. Rep. **9**, 4860–4872 (2019)
24. T. Zhou, G. Zhang, H. Zhang, H. Yang, P. Ma, X. Li, X. Qiu, G. Liu, Highly efficient visible-light-driven photocatalytic degradation of rhodamine B by a novel Z-scheme Ag_3 PO_4/MIL-101/$NiFe_2O_4$ composite. Catal. Sci. Technol. **8**, 2402–2416 (2018)
25. D. Ding, Z. Jiang, Q. Ouyang, L. Wang, Y. Zhang, L. Zan, Enhanced photocatalytic activity and mechanism insight of MnO_x/MIL-101. J. Taiwan Inst. Chem. Eng. **82**, 226–232 (2018)
26. M. Lv, H. Yang, Y. Xu, Q. Chen, X. Liu, F. Wei, Improving the visible light photocatalytic activities of $Bi_{25}FeO_{40}$/MIL-101/PTH via polythiophene wrapping. J. Environ. Chem. Eng. **3**, 1003–1008 (2015)
27. A.E. Greenberg, *Standard Methods for the Examination of Water and Wastewater* (American Public Health Association, Washington, DC, 1985)
28. L. Shen, S. Liang, W. Wu, R. Liang, L. Wu, Multifunctional NH_2-mediated zirconium metal–organic framework as an efficient visible-light-driven photocatalyst for selective oxidation of alcohols and reduction of aqueous Cr(vi). Dalt. Trans. **42**, 13649–13657 (2013)
29. T. Van Vu, H. Kosslick, A. Schulz, J. Harloff, E. Paetzold, M. Schneider, J. Radnik, N. Steinfeldt, G. Fulda, U. Kragl, Selective hydroformylation of olefins over the rhodium supported large porous metal-organic framework MIL-101. Appl. Catal. A **468**, 410–417 (2013)
30. S.M. Hosseinpour-Mashkani, F. Mohandes, M. Salavati-Niasari, K. Venkateswara-Rao, Microwave-assisted synthesis and photovoltaic measurements of $CuInS_2$ nanoparticles prepared by using metal-organic precursors. Mater. Res. Bull. **47**, 3148–3159 (2012)
31. M. Salavati-Niasari, F. Soofivand, A. Sobhani-Nasab, M. Shakouri-Arani, A. Yeganeh Faal, S. Bagheri, Synthesis, characterization, and morphological control of $ZnTiO_3$ nanoparticles through sol-gel processes and its photocatalyst application. Adv. Powder Technol. **27**, 2066–2075 (2016)
32. H. Ait Ahsaine, A. El Jaouhari, A. Slassi, M. Ezahri, A. Benlhachemi, B. Bakiz, F. Guinneton, J.R. Gavarri, Electronic band structure and visible-light photocatalytic activity of Bi_2WO_6: elucidating the effect of lutetium doping. RSC Adv. **6**, 101105–101114 (2016)

33. Y. Xu, M. Lv, H. Yang, Q. Chen, X. Liu, F. Wei, $BiVO_4$/MIL-101 composite having the synergistically enhanced visible light photocatalytic activity. RSC Adv. **5**, 43473–43479 (2015)
34. K. Fujihara, S. Izumi, T. Ohno, M. Matsumura, Time-resolved photoluminescence of particulate TiO_2 photocatalysts suspended in aqueous solutions. J. Photochem. Photobiol., A **132**, 99–104 (2000)
35. M. Ghanbari, S. Gholamrezaei, M. Salavati-Niasari, Ag_2CdI_4: synthesis, characterization and investigation the strain lattice and grain size. J. Alloys Compd. **667**, 115–122 (2016)
36. A. Jarrah, S. Farhadi, $K_6P_2W_{18}O_{62}$ encapsulated into magnetic Fe_3O_4/MIL-101 (Cr) metal-organic framework: a novel magnetically recoverable nanoporous adsorbent for ultrafast treatment of aqueous organic pollutants. RSC Adv. **8**, 37976–37992 (2018)
37. L. Nirumand, S. Farhadi, A. Zabardasti, A. Khataee, Copper ferrite nanoparticles supported on MIL-101/reduced graphene oxide as an efficient and recyclable sonocatalyst. J. Taiwan Inst. Chem. Eng. **93**, 674–685 (2018)
38. F. Motahari, M.R. Mozdianfard, F. Soofivand, M. Salavati-Niasari, NiO nanostructures: synthesis, characterization and photocatalyst application in dye wastewater treatment. RSC Adv. **4**, 27654–27660 (2014)
39. I. Langmuir, The adsorption of gases on plane surfaces of glass, mica and platinum. J. Am. Chem. Soc. **40**, 1361–1403 (1918)
40. H. Fan, X. Zhao, J. Yang, X. Shan, L. Yang, Y. Zhang, X. Li, M. Gao, ZnO-graphene composite for photocatalytic degradation of methylene blue dye. Catal. Commun. **29**, 29–34 (2012)
41. Y. Wang, R. Shi, J. Lin, Y. Zhu, Significant photocatalytic enhancement in methylene blue degradation of TiO_2 photocatalysts via graphene-like carbon in situ hybridization. Appl. Catal. B **100**, 179–183 (2010)
42. P. Du, A. Bueno-López, M. Verbaas, A.R. Almeida, M. Makkee, J.A. Moulijn, G. Mul, The effect of surface OH-population on the photocatalytic activity of rare earth-doped P25-TiO_2 in methylene blue degradation. J. Catal. **260**, 75–80 (2008)
43. A. Houas, H. Lachheb, M. Ksibi, E. Elaloui, C. Guillard, J.M. Herrmann, Photocatalytic degradation pathway of methylene blue in water. Appl. Catal. B **31**, 145–157 (2001)
44. F. Jiang, T. Yan, H. Chen, A. Sun, C. Xu, X. Wang, A g-C_3 N_4 -CdS composite catalyst with high visible-light-driven catalytic activity and photostability for methylene blue degradation. Appl. Surf. Sci. **295**, 164–172 (2014)
45. T.J. Whang, M.T. Hsieh, H.H. Chen, Visible-light photocatalytic degradation of methylene blue with laser-induced Ag/ZnO nanoparticles. Appl. Surf. Sci. **258**, 2796–2801 (2012)
46. J.Z. Kong, A.D. Li, X.Y. Li, H.F. Zhai, W.Q. Zhang, Y.P. Gong, H. Li, D. Wu, Photo-degradation of methylene blue using Ta-doped ZnO nanoparticle. J. Solid State Chem. **183**, 1359–1364 (2010)
47. Y. Wang, Y. Zhang, Z. Jiang, G. Jiang, Z. Zhao, Q. Wu, Y. Liu, Q. Xu, A. Duan, C. Xu, Controlled fabrication and enhanced visible-light photocatalytic hydrogen production of Au@CdS/MIL-101 heterostructure. Appl. Catal. B **185**, 307–314 (2016)
48. D. Channei, Fe_3O_4/SiO_2/CeO_2 core-shell magnetic nanoparticles as photocatalyst. Environ. Sci. (2014) 1–9. http://environment.scientific-journal.com
49. H. Seema, K.C. Kemp, V. Chandra, K.S. Kim, Graphene–SnO_2 composites for highly efficient photocatalytic degradation of methylene blue under sunlight. Nanotechnology **355705**, 1–8 (2012)
50. A. Elaziouti, Preparation and characterization of p–n heterojunction $CuBi_2O_4$/CeO_2 and its photocatalytic activities under UVA light irradiation. J. King Saud. Univ. Sci. **27**, 120–135 (2015)